ACS Catalysis

Research Article

pubs.acs.org/acscatalysis

Combined Spectroscopic and Theoretical Approach to Sulfur-Poisoning on Cu-Supported Ti−Zr Mixed Oxide Catalyst in the Selective Catalytic Reduction of NO_x

Jie Liu,[†] Xinyong Li,*[,†,‡,§] Qidong Zhao,[†] Ce Hao,[†] Shaobin Wang,[‡] and Moses Tadé[‡]

[†]Key Laboratory of Industrial Ecology and Environmental Engineering, Key Laboratory of Fine Chemical, School of Environmental Sciences and Technology, Dalian University of Technology, Dalian 116024, China

[‡]Department of Chemical Engineering, Curtin University, Perth, Western Australia 6845, Australia

[§]Centre for Catalysis Research, Department of Chemical Engineering, Building No. 54, Cnr Ring Road and South Lane Upper Campus, University of Cape Town, 7701 Rondebosch, South Africa

S *Supporting Information*

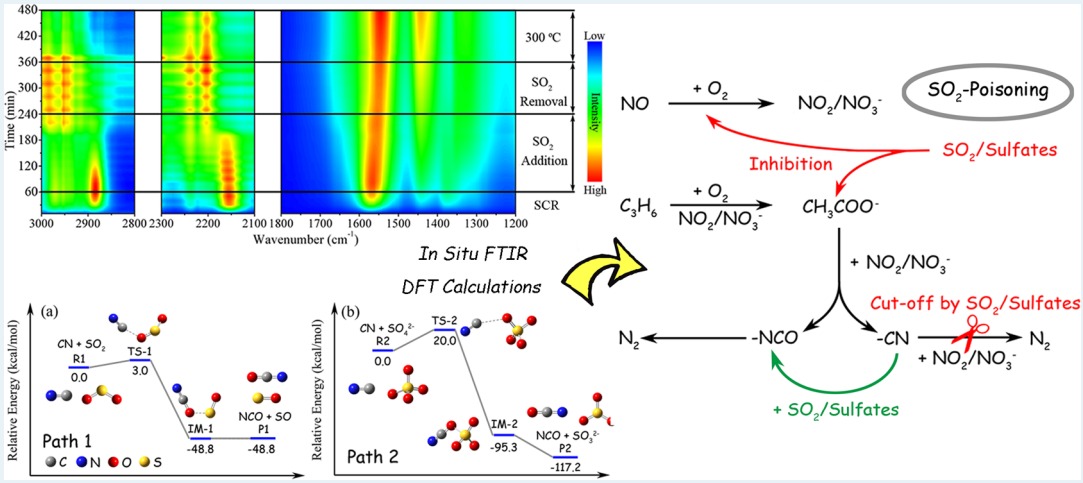

ABSTRACT: The SO_2-poisoning on a Cu-supported Ti−Zr mixed oxide catalyst ($Cu/Ti_{0.7}Zr_{0.3}O_{2-\delta}$) in selective catalytic reduction (SCR) of NO_x with C_3H_6 was investigated, and the different effects of SO_2 at varying reaction temperatures were clarified by in situ Fourier transform infrared (FTIR) spectroscopy combined with density functional theory (DFT) calculations. In situ FTIR results of the catalyst at low temperatures (150−250 °C) implied that the formation of sulfates on the surface inhibited the activation of NO and C_3H_6 as well as the reactivity of nitrates and NO_2. The weakened capacity of the catalyst toward acetate formation is an important reason for the decline of catalytic activity at low temperatures. At high temperatures (above 275 °C), the negative effect of SO_2 on the C_3H_6 activation to acetate is quite weak. More importantly, the generation of −NCO species is enhanced significantly via the reaction $-CN + SO_2/SO_4^{2-} \rightarrow -NCO$, which is confirmed by both in situ FTIR experimental observations and DFT calculations. The promotion in the generation of −NCO species is the primary reason for the elevation of SCR activity at high temperatures.

KEYWORDS: *selective catalytic reduction, SO_2-poisoning, −CN species, in situ Fourier transform infrared spectroscopy, density functional theory calculations*

INTRODUCTION

The emissions of nitrogen oxides from stationary and mobile fuel combustion sources have led to serious environmental problems, and ever-increasing environmental concerns in the last decades have spurred both academic and industrial research on the selective catalytic reduction (SCR) of NO_x.[1−4]

The SCR reaction by hydrocarbons (HCs) has attracted a lot of attention and is believed to be one of the promising ways to remove NO_x from automotive exhaust gases by taking into account the economy, energy-saving and safety.[5−9] In our previous study, we described a novel Cu-supported Ti−Zr mixed oxide catalyst ($Cu/Ti_{0.7}Zr_{0.3}O_{2-\delta}$) used for C_3H_6-SCR reaction under lean-burn conditions, and it achieved a maximum NO conversion about 80% at 275 °C.[10] Compared with the traditional Cu-based catalysts with SiO_2 or Al_2O_3 as supports, which always harvest high NO conversions above 350

Received: April 28, 2014
Revised: June 6, 2014
Published: June 16, 2014

   dx.doi.org/10.1021/cs5005739 | ACS Catal. 2014, 4, 2426−2436

°C,[11−15] the $Cu/Ti_{0.7}Zr_{0.3}O_{2-\delta}$ behaved as an excellent catalyst for low-temperature HC-SCR reaction. Due to the possible catalyst deactivation caused by SO_2, which permanently exists in typical diesel fired exhausts,[16] it is necessary to examine the tolerance capacity of the $Cu/Ti_{0.7}Zr_{0.3}O_{2-\delta}$ catalyst against SO_2 poisoning. Moreover, the mechanistic investigation of the SO_2-containing SCR reaction would be beneficial for the exploitation of new catalysts with high sulfur-resistance.

Several studies have reported competitive adsorption between SO_2 and NO, and the blockage of active sites as the mainly negative effect of SO_2 in SCR reaction.[17−19] For the HC-SCR reaction, the presence of SO_2 may affect the activation of hydrocarbons to oxygenates $C_xH_yO_z$ (formate, acetate, acetone and enolic species) and the subsequent formation and transformation of N-containing organics (R−NO, −NCO and species) formed by the reactions between oxygenates and nitrates and/or NO_2, which act as the key factors governing the SCR activity.[2,20−22]

Some reports on $Ag/\gamma-Al_2O_3$ catalysts used in C_3H_6-SCR reaction confirmed that the presence of SO_2 increases the activity and selectivity of the catalysts in the generation of −NCO species by the Ag_2SO_4 formation.[23,24] However, He et al. investigated the SO_2 poisoning on C_3H_6-SCR reaction over $Ag-Pd/Al_2O_3$ catalyst and suggested that both $Al_2(SO_4)_3$ and Ag_2SO_4 inhibit the formation of enolic, and therefore suppress the formation of surface −NCO species.[25] In the case of In/Al_2O_3 catalyst,[7] the blockage of surface oxidation sites by $Al_2(SO_4)_3$ leads to the increase of activation energies and therefore simplifies the pathway for N_2 generation via the direct reaction between the adsorbed NO_x species and the oxygenates. Whereas in the case of SO_2-free, N_2 was produced by the reaction between the activated NO_x species and the N-containing organics $C_xH_yO_zN$. Recently, a high SO_2-resistance of Zr−Nb solid solution catalyst in the C_3H_6-SCR reaction was reported by Kantcheva et al.,[26] in which a little deactivation in the flow containing a low concentration of SO_2 (56 ppm) was observed with slight activity decline of 13%. They suggested the decrease in catalytic activity to be caused by the suppression effect of SO_2 on the formation of nitroacetone and resultant hindrance on −NCO species transformation, the latter was also reported by Hadjiivanov over a Co/ZrO_2 catalyst through catalyst sulfation.[27]

However, several reports showed the promotion of SCR activity in the presence of SO_2. Li et al. reported that the low-temperature activity of C_3H_6-SCR reaction (below 250 °C) over $Ag/TiO_2-Al_2O_3$ is enhanced by the formation of surface adsorbed sulfates, which promotes the surface Lewis acidity and consequently accelerates C_3H_6 activation.[28] He[29] and Dongare[30] also agreed on the enhancement of surface acidity as an effective way to improve the SO_2-resistance of catalysts. In the study of Pt+Cu/Zr-pillared-clays catalyst, Sadykov et al.[31] suggested that the surface sulfation of the catalyst could increase the reactivity of N-containing organics by decreasing the bonding strength and coverage; hence, producing the positive effect on the SCR reaction. There have been some other reports about the SO_2-tolerance capacity of Cu-loaded catalysts in the HC-SCR reactions,[32−34] but the effect of SO_2 on the intermediates, including their generation and transformation, has not been systemically addressed.

In the present study, we examined the SO_2-poisoning on a $Cu/Ti_{0.7}Zr_{0.3}O_{2-\delta}$ catalyst in the C_3H_6-SCR reaction, and we focused on the changes of reaction mechanism caused by the presence of SO_2. The formation and transformation of intermediates during the SCR process, including nitrates, oxygenated hydrocarbons, −NCO and −CN species, were systematically studied by in situ Fourier transform infrared (FTIR) spectroscopy. Besides, the reaction pathways of the final intermediate −NCO and −CN species in the presence of SO_2 were calculated by density functional theory (DFT) due to the close relationship between their behaviors and the catalytic performance. By combining experimental observations and DFT calculations, a comprehensive mechanism for C_3H_6-SCR reaction in the presence of SO_2 over the $Cu/Ti_{0.7}Zr_{0.3}O_{2-\delta}$ catalyst was proposed.

EXPERIMENTAL SECTION

2.1. Catalyst Preparation. The $Cu/Ti_{0.7}Zr_{0.3}O_{2-\delta}$ catalyst (Cu loading was 5.0 wt %) was synthesized using an impregnation-urea precipitation method, and the details have been reported in our previous work.[10] Concisely, the $Ti_{0.7}Zr_{0.3}O_{2-\delta}$ support was synthesized using a urea precipitation method with $TiOSO_4{\cdot}2H_2O$ and $ZrOCl{\cdot}8H_2O$ as the precursors and $CO(NH_2)_2$ as the precipitator. The mixed solution was continuously stirred at 90 °C for 8 h. After filtration and washing, the obtained precipitant was dried and then calcined at 400 °C for 4 h. The $Cu/Ti_{0.7}Zr_{0.3}O_{2-\delta}$ catalyst was prepared using a wet impregnation method with $Cu(NO_3)_2$ solution. The catalyst was dried and then calcined at 400 °C for 4 h.

2.2. Catalytic Activity Tests. The SCR activity measurement was carried out in a fixed-bed quartz tube reactor (6 mm internal diameter) containing 200 mg of catalyst (40−60 mesh). Prior to an experiment, the catalyst was pretreated at 250 °C for 1 h in an Ar stream, and the activity test was performed from 150 to 350 °C at a heating rate of 10 °C/min. The typical composition of reactant gases was as follows: $[NO] = [C_3H_6]$ = 1000 ppm, $[O_2]$ = 2.5 vol %, $[SO_2]$ = 150−600 ppm (when used), $[H_2O]$ = 10 vol % (when used), and He as the balance. The total flow rate was 100 mL/min, which corresponded to an hourly space velocity (GHSV) of approximately 30 000 h^{-1}. The concentrations of NO, NO_2, CO and CO_2 in the inlet and outlet gases were measured using a chemiluminescence gas analyzer (Testo 350). The concentrations of N_2, N_2O and C_3H_6 were analyzed using a gas chromatograph (Agilent 7890A), and the corresponding columns were 5A molecular sieve and Paropak Q columns with a thermal conductivity detector (TCD) and a 6X-104D column with a flame ionization detector (FID), respectively.

2.3. In Situ FTIR Study. The formation and transformation of adsorbed species on the catalyst surface under different reaction conditions were investigated by in situ FTIR spectra, using a FTIR spectrometer Bruker Vertex 70-FTIR. Prior to each experiment, the sample (~20 mg) was pretreated in a He stream (50 mL/min) at 250 °C for 1 h. If there is no special annotation, the in situ FTIR spectrum for each measurement was all selected when the surface adsorbed species achieved the steady state in 60 min and no change of the spectra was observed. All IR spectra were recorded in accumulative 64 scans with a resolution of 4 cm^{-1} in the range of 4000−400 cm^{-1}. The concentrations of NO, C_3H_6, SO_2 and O_2 in the gas mixture were 1000, 1000, 600 ppm and 2.5 vol % (when used), respectively, and He as the balance. The flow rate of mixed gas was 50 mL/min.

2.4. Computational Methods. The Gaussian 09 programs were used to perform an investigation of the potential energy surface of the reactions. All the reactants, products, intermediates and transition states were optimized using the hybrid density functional B3LYP method and the 6-311 G (d, p) basis set.[35] Vibrational analysis verified the identity of each stationary point as either a minimum or transition state. The zero-point energy (ZPE) corrections were performed at the same level of theory. Intrinsic reaction coordinates (IRC) calculations were used to link each transition state structure with corresponding intermediate geometries to develop an energy profile.

RESULTS AND DISCUSSION

3.1. Effects of SO_2 on Catalytic Activity and Stability. The effects of SO_2 on NO conversion and N_2 yield over Cu/

dx.doi.org/10.1021/cs5005739 | ACS Catal. 2014, 4, 2426−2436

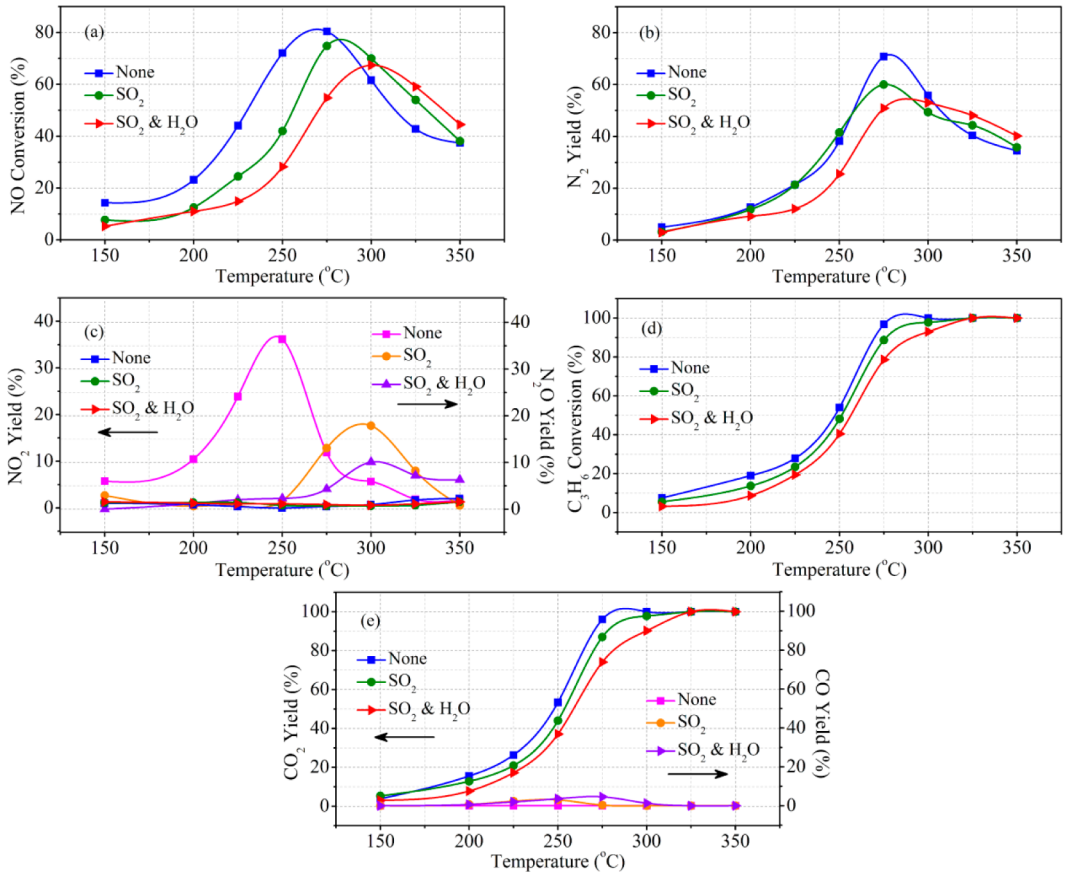

Figure 1. C_3H_6–SCR performance of $Cu/Ti_{0.7}Zr_{0.3}O_{2-\delta}$ catalyst at various temperatures under different reaction conditions, including the standard, the SO_2-containing, and the SO_2 and H_2O-containing C_3H_6-SCR reactions. (a) NO conversion, (b) N_2 yield, (c) N_2O and NO_2 yield, (d) C_3H_6 conversion and (e) CO_2 and CO yield. Conditions: [NO] = [C_3H_6] = 1000 ppm, [O_2] = 2.5 vol %, [SO_2] = 150 ppm (when used), [H_2O] = 10 vol % (when used), and He as the balance.

$Ti_{0.7}Zr_{0.3}O_{2-\delta}$ catalyst are presented in Figure 1a,b, respectively. Compared with the standard SCR reaction, SO_2 introduction inhibited the low-temperature activity (150–250 °C) of the catalyst to some extent and caused a slight decrease of the maximum NO conversion obtained at 275 °C, from 80.4% to 74.8%. The suppression of N_2 formation by SO_2 within the same temperature range was not as evident as that of NO conversion, though the maximum N_2 yield also declined from 70.8% to 60.0%. At the higher temperatures, the presence of SO_2 increased the NO conversion by approximatly 11% at 300 and 325 °C, and the N_2 yield obtained at 325 °C was also enhanced slightly. Figure 1c compares the N_2O yield over the $Cu/Ti_{0.7}Zr_{0.3}O_{2-\delta}$ catalyst in the absence and the presence of SO_2. In the SO_2-free flow, there was a significant N_2O yield in the temperature range of 150–250 °C, which was enhanced quickly by raising the temperature and achieved the maximum of 36.4% at 250 °C. With further increasing the temperature, the generation of N_2O was weakened significantly and almost no N_2O was produced at 350 °C. For the SO_2-containing case, the temperature for N_2O generation was elevated evidently, which resulted in the negligible N_2O yield in the temperature range of 150–250 °C. The maximum N_2O yield of 17.8% was obtained at 300 °C, and it was much lower than that of 36.4% in the SO_2-free case. The formation of N_2O was not detected when the reaction temperature was raised up to 350 °C. Figure 1c also implied that the NO_2 production was quite low both in the absence and the presence of SO_2.

For the C-containing species, the SO_2 introduction caused a slight decrease of C_3H_6 conversion, as described in Figure 1d. The negative effect of SO_2 on C_3H_6 activation may result in the decline of SCR activity at low temperatures, whereas it may promote the deNO$_x$ efficiency at high temperatures due to the less consumption of C_3H_6 via complete oxidation, which was the main side reaction of SCR at high temperatures. From Figure 1e, it was suggested that CO_2 was the main C-containing product, and the presence of SO_2 led to the generation of some CO. From the production profiles, it was indicated that the presence of SO_2 mainly affected the generation of N_2O as well as the conversion of C_3H_6, and the improvement of reaction activity was mainly caused by the enhancement of N_2O yield. In previous reports,[36,37] the condition for a catalyst with better combustion activity benefits the N_2O production. Herein, it could be the restraint of C_3H_6 combustion by SO_2, which caused the elevation of temperature for N_2O generation and the consequent higher N_2O yield was obtained only above 275 °C. On the other hand, the suppression of N_2O formation caused by SO_2 introduction was the primary reason for the decline of NO conversion in the temperature range of 150–250 °C, whereas the negative effect of SO_2 on N_2 and NO_2 yields was quite weak.

Due to the definite presence of certain amounts of H_2O in the actual exhaust, the activity of the $Cu/Ti_{0.7}Zr_{0.3}O_{2-\delta}$ catalyst in the coexistence of SO_2 and H_2O has also been tested, and the results are displayed in Figure 1. The SO_2 and H_2O-containing atmosphere led to a further decrease of the low-

dx.doi.org/10.1021/cs5005739 | ACS Catal. 2014, 4, 2426–2436

temperature activity of the catalyst. Whereas, similar to the SO_2-containing condition, when the temperature was raised above 275 °C, the NO conversion and N_2 yield were both enhanced, which were even a little higher than those obtained in the SO_2-containing SCR reaction. The introduction of H_2O inhibited the formation of N_2O slightly, leading to the lower N_2O yields compared with those in the SO_2-containing reaction, but did not affect the NO_2 yields, which were also pretty low at various temperatures. Meanwhile, the presence of SO_2 and H_2O further suppressed the complete oxidation of C_3H_6, leading to the lowest C_3H_6 conversion and CO_2 yield, as well as the highest CO yield, among the three reaction conditions. From Figure 1, it was indicated that the coexistence of SO_2 and H_2O aggravated the catalyst deactivation in the temperature range of 150−250 °C slightly, but the catalytic performance at high temperatures was quite similar to that in the SO_2-containing reaction. Herein, we considered the presence of SO_2 as the most important factor for the deactivation of the catalyst, and we mainly discussed the effect of SO_2 on the C_3H_6-SCR reaction over the $Cu/Ti_{0.7}Zr_{0.3}O_{2-\delta}$ catalyst in the present study.

Moreover, we have compared the X-ray diffraction (XRD) patterns of the fresh catalyst and the used catalysts after the SO_2-containing and SO_2 and H_2O-containing reactions, and the results are presented in Figure S1 in the Supporting Information. By comparison, there was no new characteristic peak corresponding to any sulfate species or aggregate actives species over the used catalysts. The highly similar XRD patterns of the three samples suggested the weak sulfation of catalyst as well as the high structure stability of catalyst.

The durability of $Cu/Ti_{0.7}Zr_{0.3}O_{2-\delta}$ and the SO_2-ponsioning on this catalyst have been tested and the results are presented in Figure 2. As presented in Figure 2a, the catalyst exhibited

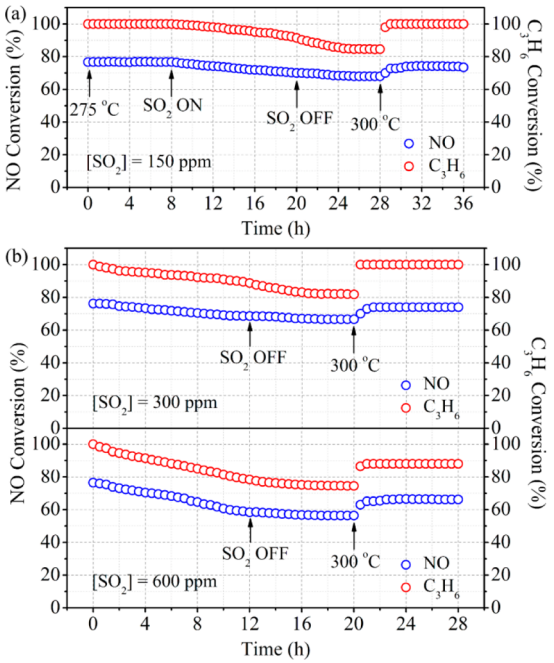

Figure 2. (a) Stability of $Cu/Ti_{0.7}Zr_{0.3}O_{2-\delta}$ catalyst and the effect of SO_2 addition on SCR performance at 275 °C; (b) effect of SO_2 concentration on SCR performance over $Cu/Ti_{0.7}Zr_{0.3}O_{2-\delta}$ catalyst. Conditions: [NO] = [C_3H_6] = 1000 ppm; [O_2] = 2.5 vol %; [SO_2] = 150−600 ppm (when used); He as the balance.

high stability in the initial reaction gases without SO_2 at 275 °C for 8 h. After the introduction of SO_2 at 150 ppm, NO conversion declined gradually from 76.8% to 70.0% after 12 h, and the corresponding C_3H_6 conversion declined gradually from 100% to 90.3%. Because no NO and C_3H_6 conversions were restored after SO_2 removal, the SO_2 poisoning on the catalyst could be irreversible. However, the C_3H_6 conversion on the same catalyst could be recovered to 100% by increasing the reaction temperature to 300 °C, and the corresponding NO conversion almost achieved the previous level obtained in the SO_2-free stream (~77%). The deactivation of the $Cu/Ti_{0.7}Zr_{0.3}O_{2-\delta}$ catalyst caused by SO_2 with different concentrations was also tested, and the results are presented in Figure 2b. The performance of the catalyst in the SCR reaction containing 300 ppm of SO_2 was similar to that containing 150 ppm of SO_2 (Figure 2a). Both of the NO and C_3H_6 conversions declined after a reaction time of 12 h, and the SO_2-poisoning on the catalyst was irreversible, though the catalytic activity could be recovered by increasing the reaction temperature. By a comparison, the high concentration SO_2 (600 ppm) resulted in a more obvious deactivation of the catalyst, and only partial activity could be recovered by raising the temperature to 300 °C.

3.2. Effect of SO_2 on Reactants Adsorption and Oxidation.

3.2.1. Effect of SO_2 on NO Adsorption and Oxidation. In the SCR process, the adsorbed nitrates and NO_2 deriving from NO oxidation are widely believed to be the precursors for the generation of −NCO and −CN species, and they are also thought to participate in the reaction of N_2 formation.[38−40] Herein, the effect of SO_2 on NO adsorption and oxidation over the $Cu/Ti_{0.7}Zr_{0.3}O_{2-\delta}$ catalyst has been studied by in situ FTIR. Figure 3 presents the changes of IR spectra caused by the switch of reaction gas between NO + O_2 and SO_2 + O_2 over the $Cu/Ti_{0.7}Zr_{0.3}O_{2-\delta}$ catalyst at 275 °C. For a fresh sample (Figure 3a), the catalyst surface was mainly covered by various nitrates during the NO + O_2 coadsorption, including bridging nitrates (1605−1615 cm^{-1}), bidentate nitrates (1230−1245 and 1575−1585 cm^{-1}) and monodentate nitrates (1280−1295 and 1558 cm^{-1}).[41−47] The bands around 1283 and 1445 cm^{-1} were assigned to the nitrites, which provided evidence for the stabilization of NO_2 on the catalyst surface.[22,48,49] Moreover, the band around 1349 cm^{-1} was assigned to the NO_2 stretch of a distorted $(NO_3^-)_2$;[50] on the other hand, this band could also be the characteristic band of sulfates in the presence of SO_2.[51] These nitrates and nitrites were considered to be bound to the catalyst surface strongly as the subsequent He purging resulted in only a slight decrease in the intensity of the related absorption bands. When the reaction gas was switched to SO_2 + O_2, the sulfates deriving from SO_2 oxidation were deposited on the catalyst surface, leading to the appearance of the characteristic band of ν_s(S═O) at 1276 cm^{-1} and the intensity enhancement of the band of ν_{as}(S═O) at 1349 cm^{-1}, which was overlapped with that of distorted $(NO_3^-)_2$.[51,52] During the SO_2 + O_2 purging, the intensity of some characteristic bands related to nitrates (1235 and 1609 cm^{-1}) was decreased distinctly, while the other bands centered at 1445, 1558, and 1580 cm^{-1} still maintained the high intensity. The changes of IR spectra implied the partial occupation of adsorption sites by sulfates.

The competitive adsorption between NO and SO_2 was more remarkable on a SO_2-aged sample, as revealed in Figure 3b. The characteristic response of the nitrates on the SO_2-aged catalyst (curve III in Figure 3b) was much weaker than that on a fresh

dx.doi.org/10.1021/cs5005739 | ACS Catal. 2014, 4, 2426−2436

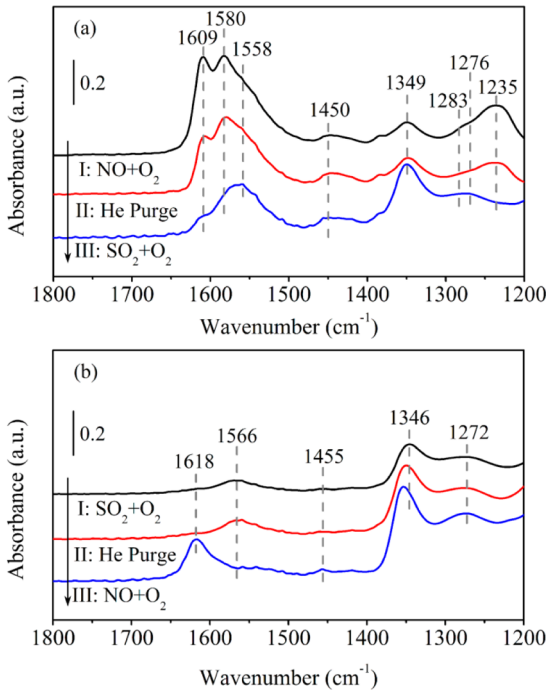

Figure 3. (a) IR spectra of the sulfates formed on the NO + O_2 pretreated Cu/$Ti_{0.7}Zr_{0.3}O_{2-\delta}$ catalyst at 275 °C; (b) IR spectra of the species deriving from NO + O_2 coadsorption on the SO_2-aged Cu/$Ti_{0.7}Zr_{0.3}O_{2-\delta}$ catalyst at 275 °C. Conditions: [NO] = 1000 ppm (when used); [O_2] = 2.5 vol %; [SO_2] = 600 ppm (when used); He as the balance.

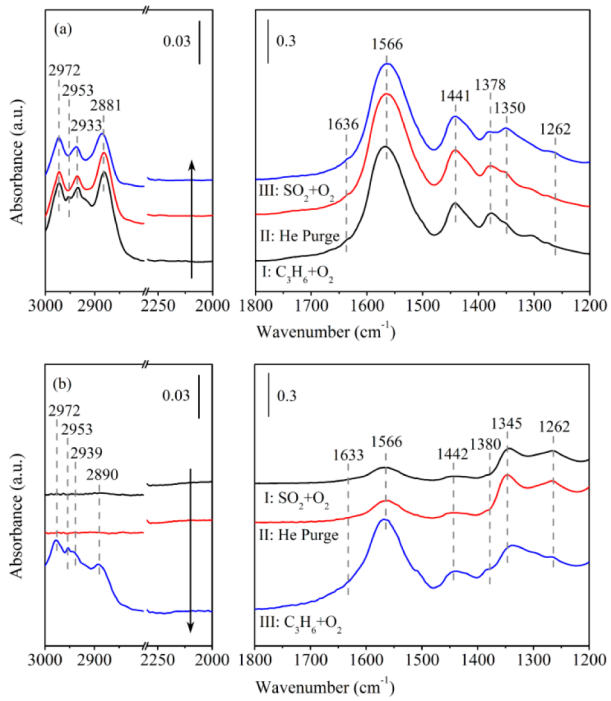

Figure 4. (a) IR spectra of the sulfates formed on the C_3H_6 + O_2 pretreated Cu/$Ti_{0.7}Zr_{0.3}O_{2-\delta}$ catalyst at 275 °C; (b) IR spectra of the species deriving from C_3H_6 activation on a SO_2-aged Cu/$Ti_{0.7}Zr_{0.3}O_{2-\delta}$ catalyst at 275 °C. Conditions: [C_3H_6] = 1000 ppm (when used); [O_2] = 2.5 vol %; [SO_2] = 600 ppm (when used); He as the balance.

one (curve I in Figure 3a). Herein, it was suggested that the SO_2-aging made the sulfates be adsorbed on the catalyst surface and occupy the adsorption sites toward nitrates preferentially. As no distinct elimination of sulfates was caused by He purging, it was implied that the sulfates were bound to the catalyst surface strongly, probably leading to an irreversible blockage of active sites, which was consistent with the analysis in Figure 2. These deductions about the negative effect of SO_2 on NO oxidation and activation were in also agreement with previous reports.[51,53] In addition, this inhibition effect existed in the whole temperature range (150−350 °C), which is supported by the results presented in Figure S2 (Supporting Information).

3.2.2. Effect of SO_2 on C_3H_6 Adsorption and Oxidation. Figure 4 presents the IR spectral changes caused by the switch of reaction gas between C_3H_6 + O_2 and SO_2 + O_2 over the Cu/$Ti_{0.7}Zr_{0.3}O_{2-\delta}$ catalyst at 275 °C. As shown in Figure 4a, coadsorption of C_3H_6 + O_2 on the fresh catalyst resulted in the generation of oxygenated hydrocarbons, including acetate ($\nu_s(COO^-)$ around 1441 cm^{-1} and $\nu_{as}(COO^-)$ around 1566 cm^{-1}) and formate ($\nu_s(COO^-)$ around 1350 cm^{-1}, $\delta(CH)$ around 1378 cm^{-1} and $\nu_{as}(COO^-)$ around 1566 cm^{-1}), whereas the band at 1636 cm^{-1} was assigned to $\delta(OH)$ of H_2O.[54−56] The following successive purging of He and SO_2 + O_2 gas decreased the concentrations of formate and acetate weakly, implying the strong interaction between these oxygenates and the catalyst surface as well as the weak competitive adsorption between C_3H_6 and SO_2.

The suppression of C_3H_6 activation caused by surface adsorbed sulfates can be observed on the SO_2-aged Sample, as presented in Figure 4b. Comparing curve III in Figure 4b and curve I in Figure 4a, the band attributed to formate around 1380 cm^{-1} almost vanished on the SO_2-aged sample, and the intensity of the band centered at 1441 cm^{-1} assigned to acetate was also weakened slightly in the meantime. This inhibition effect can be seen more clearly from the spectra in the range of 3000−2800 cm^{-1}, where the bands centered at 2881 and 2953 cm^{-1} were attributed to $\nu_s(CH)$ and $\nu_{as}(COO)$ + $\delta(CH)$ of formate, and the bands around 2933 and 2972 cm^{-1} were assigned to $\nu_s(COO^-)$ and $\nu_s(CH)$ of acetate, respectively.[44,56]

By investigating the effect of reaction temperature on SO_2 poisoning for C_3H_6 activation (Figure S3 in the Supporting Information), it was implied that the inhibition effect of SO_2 was alleviated by raising the temperature. Especially, when the reaction temperate was above 275 °C, the formation of acetate was promoted significantly. Considering the high activity of acetate in the reaction with nitrates,[44,57] it was indicated that the activity decline in the temperature range of 150−250 °C could be attributed to the weakened capacity of catalyst in the activation of C_3H_6 to acetate. Whereas with the abating negative effect of SO_2 on the acetate generation by raising the temperature, the SCR activity of the catalyst was recovered, and even enhanced.

3.3. Effect of SO_2 on SCR Process. The effect of SO_2 on the surface adsorbed species during the SCR process has been studied in detail by in situ FTIR and the results are presented in Figure 5. In the SO_2-free SCR reaction (Figure 5a), the partially oxidized hydrocarbons were generated on the catalyst surface from 150 °C, including formate (1349, 1386 and 1544 cm^{-1}), acetate (1441 and 1544 cm^{-1}) and acetone (ν (C═O) around 1667 cm^{-1}),[44] and their concentrations were enhanced by increasing reaction temperature. Meanwhile, the intensity of the characteristic bands assigned to various nitrates (1244, 1283, 1418, 1581 and 1610 cm^{-1}), NO_2 (1283 cm^{-1}) and adsorbed mononitrosyl (1845 and 1905 cm^{-1})[48] was decreased gradually,

dx.doi.org/10.1021/cs5005739 | ACS Catal. 2014, 4, 2426−2436

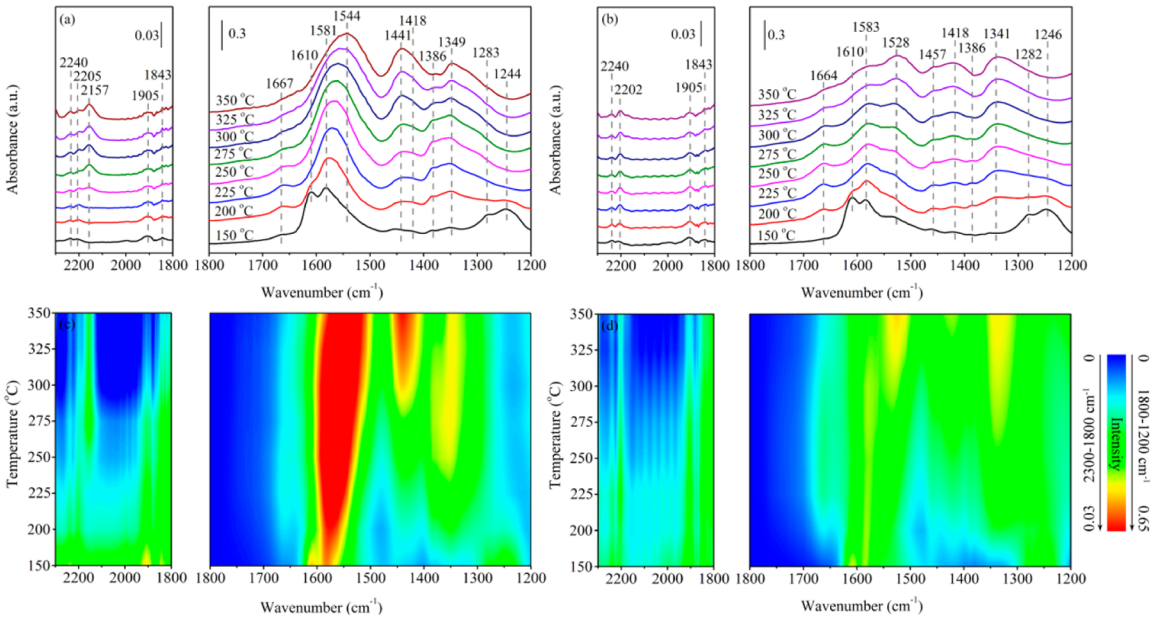

Figure 5. IR spectra of surface species formed during C_3H_6-SCR reaction at various temperatures over the $Cu/Ti_{0.7}Zr_{0.3}O_{2-\delta}$ catalyst in the absence of SO_2 (a) and in the presence of SO_2 (b). Conditions: [NO] = [C_3H_6] = 1000 ppm; [O_2] = 2.5 vol %; [SO_2] = 600 ppm (when used); He as the balance.

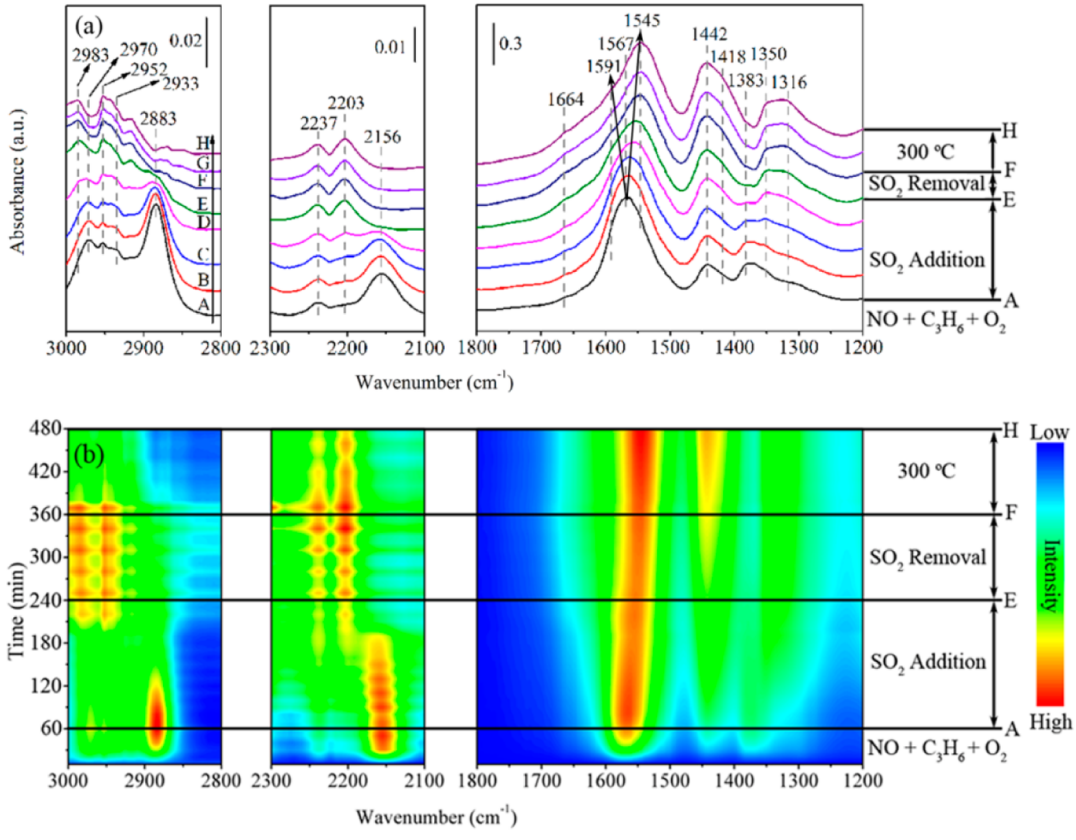

Figure 6. Dynamic changes of in situ FTIR spectra caused by the SO_2 addition over $Cu/Ti_{0.7}Zr_{0.3}O_{2-\delta}$ catalyst at 275 °C. A, NO + C_3H_6 + O_2 for 60 min; B−E, NO + C_3H_6 + O_2 + SO_2 for 30, 60, 120 and 180 min; F, removal of SO_2 for 120 min; G−H, increasing temperature to 300 °C for 30 and 120 min. Conditions: [NO] = [C_3H_6] = 1000 ppm; [O_2] = 2.5 vol %; [SO_2] = 600 ppm (when used); He as the balance.

which was caused by the enhancement of their reaction with oxygenates as well as the thermal decomposition. Then the reaction between oxygenates and nitrates and/or NO_2 induced the generation of −NCO (2205 and 2240 cm^{-1}) and −CN species (2157 cm^{-1}),[21,58,59] and the band around 2157 cm^{-1} only appeared at high temperatures (above 250 °C). Moreover, as C_3H_6 may be oxidized to CO during the SCR reaction, the possibility of CO adsorption on the catalyst surface could not be excluded totally, which may result in the IR response at around 2150 cm^{-1}.

dx.doi.org/10.1021/cs5005739 | ACS Catal. 2014, 4, 2426−2436

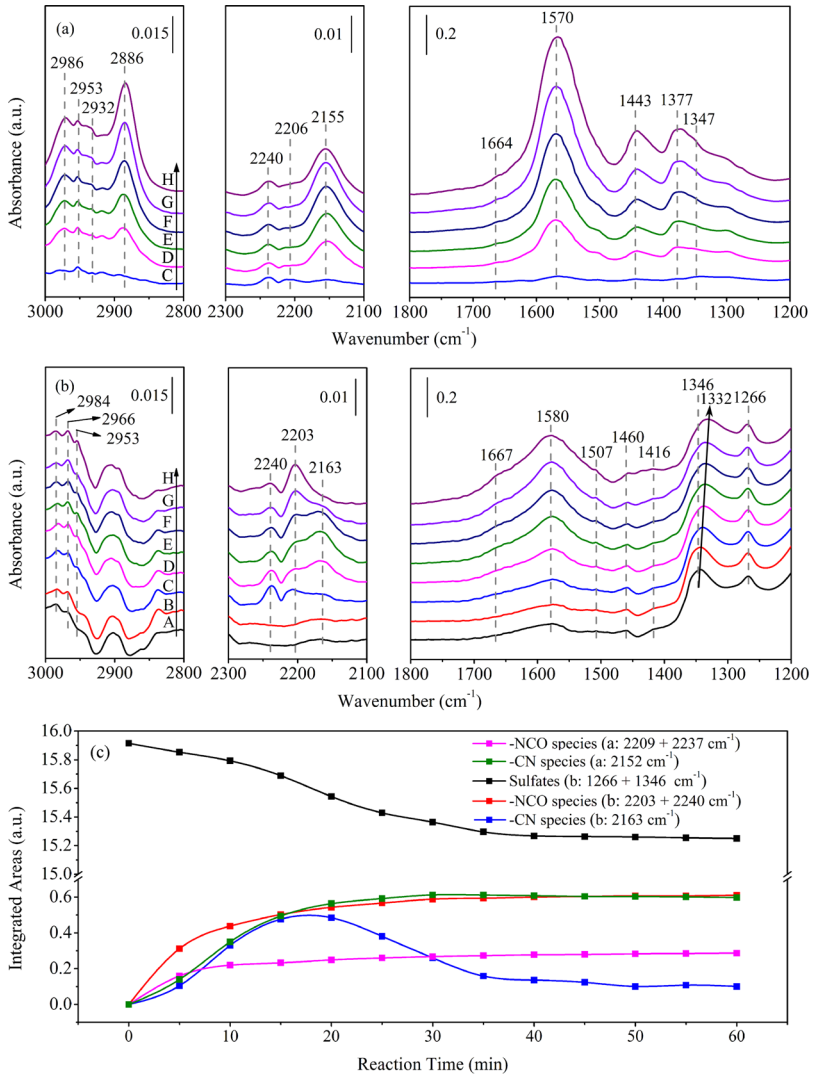

Figure 7. Dynamic changes of the in situ FTIR spectra as a function of time at 275 °C over the fresh (a) and SO_2-aged (b) $Cu/Ti_{0.7}Zr_{0.3}O_{2-\delta}$ catalysts. A, SO_2 + O_2 for 60 min; B, He purging for 60 min; C−H, NO + C_3H_6 + O_2 for 5, 10, 15, 20, 30, 60 min. (c) Time dependence of the integrated areas of the peaks assigned to −NCO, −CN and sulfates in panels a and b, respectively. Conditions: [NO] = [C_3H_6] = 1000 ppm; [O_2] = 2.5 vol %; [SO_2] = 600 ppm (when used); He as the balance.

To account for the band centered at 2157 cm^{-1}, we have measured the IR changes of this band under O_2-rich condition (2.5 vol % O_2) at 275 °C, and the results are presented in Figure S4 (Supporting Information). In the previous reports,[60−63] Cu-containing catalysts usually exhibited high activity in the CO oxidation reaction, which could obtain a CO conversion of 70% or higher around 275 °C. However, as described in Figure S4 (Supporting Information), the decline rate of the band intensity of 2157 cm^{-1} was quite slow even at the high temperature of 275 °C, implying the poor reactivity of these species with O_2. Herein, the band centered at 2157 cm^{-1} could not be only due to the adsorption of CO, and we assigned this band to the overlapped band of CO and −CN species, in particular, the −CN species were considered as the main adsorption species.

Compared with the SO_2-free case (Figure 5a), the intensity of the bands assigned to nitrates and oxygenates was decreased in the SO_2-containing atmosphere, as presented in Figure 5b, suggesting the weaker capacity of the catalyst toward NO and C_3H_6 activation. Moreover, the reactivity of nitrates was lowered. As described in Figure 5b, the features of nitrates (1418, 1583 and 1610 cm^{-1}) still existed on the catalyst surface even at a reaction temperature up to 350 °C, while these nitrates were almost exhausted on the SO_2-free condition at the same temperature. For the N-containing organic intermediates, it was interesting that the characteristic band of −CN species vanished in the SO_2-containing atmosphere, while the generation of −NCO species was promoted in the meantime. We suggest two possible reasons for this phenomenon: (i) the presence of SO_2 restrained the formation of −CN species, leading to more oxygenates and nitrates and/or NO_2 to react with each other and promote the generation of −NCO species; (ii) the −CN species acting as a precursor reacting with SO_2 and/or sulfates to generate −NCO species. The formation and transformation of −CN species in the SO_2-containing atmosphere are clarified below.

3.4. Effect of SO_2 on the Formation and Transformation of Intermediates. The changes of intermediates caused by SO_2 introduction have been studied by in situ FTIR and the results are presented in Figure 6. In the SO_2-free reaction gas (curve A), the formate, acetate, acetone, −NCO and −CN species were generated, while the features of nitrates

dx.doi.org/10.1021/cs5005739 | ACS Catal. 2014, 4, 2426−2436

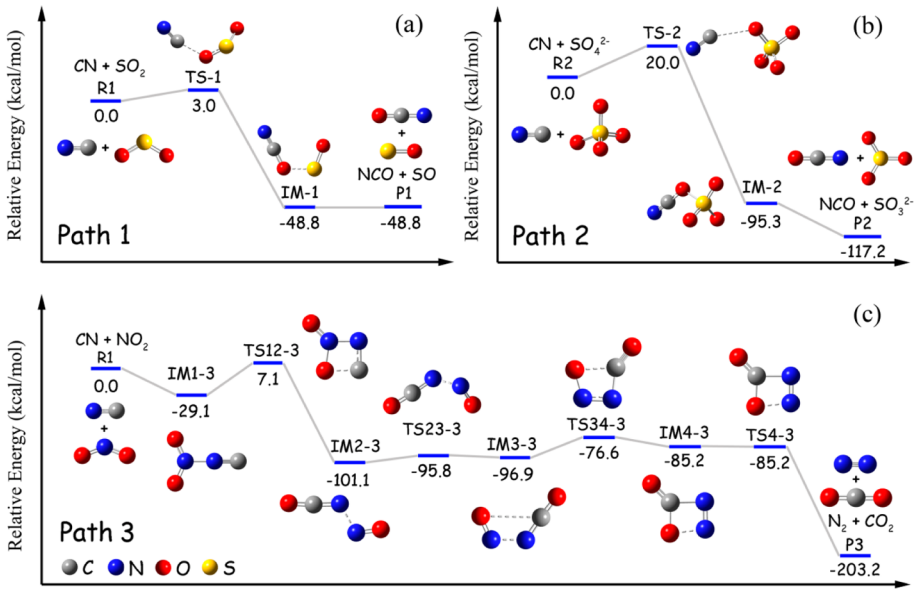

Figure 8. Schematic potential energy surface of the −CN + SO_2 (a), −CN + SO_4^{2-} (b) and −CN + NO_2 (c)[64] reactions (with inclusion of the B3LYP/6-311 G (d, p) zero-point energy (ZPE)).

were absent on the catalyst surface due to their high reactivity at 275 °C. After the SO_2 introduction, sulfates were formed and accumulated with the reaction time, enhancing the intensity of the band around 1350 cm^{-1} (curves B−E). The band at 1567 cm^{-1} was split into two bands, the band assigned to $\nu_{as}(COO^-)$ of formate and acetate (1545 cm^{-1}) and the shoulder band attributed to bidentate nitrates (1591 cm^{-1}). The regeneration of water-solved nitrates (1316 and 1418 cm^{-1})[43] suggested the weakened reactivity of nitrates. Meanwhile, the concentrations of formate (1383 and 2883 cm^{-1}) and −CN species (2156 cm^{-1}) were decreased gradually and finally vanished after 180 min (curve E), while the generation of −NCO species (2203 and 2237 cm^{-1}) was promoted significantly. Figure 6b more clearly describes the red shift of the band at 1567 cm^{-1} and the concentration changes of the nitrates, formate, −NCO and −CN species. In our previous study,[64] ,the −CN species was stable in the C_3H_6 + O_2 flow, while the hydrolysis of −NCO species forming NH_3 was observed in the meantime, which indicated that the hydrolysis of −CN species hardly occurred over the $Cu/Ti_{0.7}Zr_{0.3}O_{2-\delta}$ catalyst. Herein, it was suggested that the observed consumption of −CN species was caused by its reaction with some species, but not the hydrolysis reaction. The suppression on the reactivity of nitrates and the generation of formate and −CN species by SO_2 was irreversible, because the SO_2 removal caused little changes in the intensity of the corresponding characteristic bands. In contrast, the negative effect of SO_2 on the formation of acetate and acetone was quite weak. As presented in Figure 6, the intensities of acetate and acetone (1442 and 1664 cm^{-1}) were rising with the reaction time, even in the presence of SO_2, and the subsequent removal of SO_2 resulted in more significant enhancement of the IR response. After the temperature increased to 300 °C (curves G−H), the intensity of the bands assigned to acetate, acetone and −NCO species was further strengthened. Herein, the recovery of SCR activity at 300 °C presented in Figure 2 could be attributed to the enhancement of C_3H_6 activation and the acceleration of the −NCO species generation.

The dynamic IR spectra obtained in the stream of NO + C_3H_6 + O_2 over the fresh and SO_2-aged $Cu/Ti_{0.7}Zr_{0.3}O_{2-\delta}$ catalysts at 275 °C are represented in Figure 7a,b, respectively. The oxygenated hydrocarbons (formate, acetate and acetone), −NCO and −CN species were generated on both samples in the flow of NO + C_3H_6 + O_2. The SO_2-aging led to the appearance of sulfates features around 1266 and 1346 cm^{-1}, as described in Figure 7b. Due to the SO_2-poisoning for C_3H_6 activation, the intensity of characteristic bands of oxygenates was weaker on the SO_2-aged catalyst compared with that on the fresh one. It was worth noting that, the feature of −CN species similarly appeared on both the fresh sample and SO_2-aged catalyst, though it was not observed in the SO_2-containing SCR reaction (Figure 5b), which suggested that the SO_2-aging did not cut off the generation of −CN species. However, the SO_2-aging made the −CN species exhibit a much different behavior from that on the fresh catalyst. The −CN species on the SO_2-aged sample was consumed much rapidly after 20 min when the quantity of −CN species achieved the maximum. Moreover, there was a distinct red shift on the sulfates feature, from 1346 cm^{-1} to a lower wavenumber 1332 cm^{-1}, suggesting the probable consumption of sulfates.

In order to clarify the effect of sulfates on the transformation of −NCO and −CN species, we have integrated the peak areas assigned to −NCO, −CN and sulfates on the two samples representing the quantity of these species, and the results are presented in Figure 7c. For both of the two samples, the amount of −CN species increased with the reaction time until achieving a maximum at 20 min and then the amount decreased. By comparison, the consumption of −CN species on the SO_2-aged catalyst was much faster than that on the fresh sample, and the −CN species almost vanished after 60 min. Meanwhile, the generation of −NCO species on the SO_2-aged catalyst was accelerated remarkably, accompanied by the gradual consumption of surface adsorbed sulfates. On the basis of the results presented in Figure 7, it was inferred that the adsorbed sulfates did not prevent the generation of −CN species but changed its reaction path. The sulfates could react with −CN species and therefore promoted the formation of −NCO species. Moreover, the consumption of sulfates might release some adsorption sites for gas-phase NO, and the

dx.doi.org/10.1021/cs5005739 | ACS Catal. 2014, 4, 2426−2436

consequent enhancement in the formation of nitrates may also benefit the production of −NCO species.

3.5. DFT Studies on the Reaction Routes of −CN Species. Due to the in situ FTIR observations, the enhancement of the generation of −NCO species at the SO_2-containing atmosphere was always accompanied by the disappearance or consumption of −CN species. Herein, −CN + SO_2 → −NCO + SO and −CN + SO_4^{2-} → −NCO + SO_3^{2-} were considered as the most possible reaction routes of −CN species. The energy profiles of the two reactions have been calculated by DFT, and the results are presented in Figure 8a,b. The energy diagram depicting the reaction −CN + NO_2 → N_2 + CO_2 is presented in Figure 8c for comparison, which has been demonstrated as the most feasible reaction channel of −CN species over the $Cu/Ti_{0.7}Zr_{0.3}O_{2-\delta}$ catalyst in the SO_2-free SCR reaction in our previous study.[64] The optimized geometries of the reactants, products, intermediates and transition states in the reactions of CN + SO_2, CN + SO_4^{2-} and CN + NO_2 are presented in Figure S5 (Supporting Information). As the −CN species were confirmed to be inert in the atmosphere of O_2 or NO alone by IR spectra in the above-mentioned study,[64] the possibility that −CN species reacted with O_2 or NO to form −NCO species was excluded. As displayed by Figure S6 in the Supporting Information, the XRD pattern of the $Cu/Ti_{0.7}Zr_{0.3}O_{2-\delta}$ catalyst was much different from those of the Cu/TiO_2 and Cu/ZrO_2 catalysts, which exhibited only a broad diffraction peak with quite weak intensity. This phenomenon was caused by the partial substitution of Ti atoms by Zr atoms in the $Cu/Ti_{0.7}Zr_{0.3}O_{2-\delta}$ catalyst, which significantly inhibited the individual crystal nucleus growing of TiO_2 and ZrO_2, consequently leading to the highly amorphous and poorly crystalline states of the catalyst. Similar viewpoints have also been reported by other studies concerning the Ti-based mixed oxide materials.[65,66] Due to the complex and disordered structure of $Cu/Ti_{0.7}Zr_{0.3}O_{2-\delta}$, it was difficult to establish accurate models of the catalyst with surface adsorbed species. Alternatively, only the gas phase reactions were simulated in the present study.

Figure 8a presents the energy profile of the −CN + SO_2 reaction, in which the C atom of the −CN species attacks the O atom of SO_2 (Path 1). The combination of −CN radicals and SO_2 proceeds with an energy barrier of 3.0 kcal/mol and produces an intermediate IM-1 as the initially formed and energized adduct. Then the IM-1 directly dissociates into NCO + SO products (P1) by simply breaking the O−S bond without a barrier, which possesses the energy of −48.8 kcal/mol relative to the reactants. Due to the low activation energy of 3.0 kcal/mol, this reaction could take place easily, even in a low temperature region, which well explains the absence of −CN species and the enhancement of the −NCO species generation in the whole temperature range of 150−350 °C, as presented in Figure 5b. The calculation results about the reaction of −CN + SO_2 → −NCO + SO was similar to that reported by Hershberger et al.[67]

Figure 8b describes the energy profile of the reaction between −CN and SO_4^{2-} species, in which the C atom of −CN species attacks the O atom of SO_4^{2-} (Path 2). The reaction between −CN and SO_4^{2-} results in the generation of NCO + SO_3^{2-} products (P2) by overcoming the energy barrier of 20.0 kcal/mol from R2 to TS-2 and the consequent dissociation of intermediate IM-2. The energy of NCO + SO_3^{2-} is −117.2 kcal/mol relative to the reactants −CN + SO_4^{2-}, and the dissociation of IM-2 needs no excess energy.

Path 3 describes the reaction of −CN + NO_2 in which the N atom of species attacks the N atom of NO_2. The reactants −CN and NO_2 can evolve into N_2 + CO_2 products (P3) via a series of steps as −CN + NO_2 (R3) → IM1-3 → TS12-3 → IM2-3 → TS23-3 → IM3-3 → TS34-3 → IM4-3 → TS4-3 → N_2 + CO_2 (P3). The rate-determining step in this cycle appears to be the transfer of the first intermediate IM1-3 to the first transition state TS12-3, surmounting an energy barrier of 36.2 kcal/mol. From the energy profiles of the three reactions, we see that Paths 1 and 2 are more kinetically feasible than Path 3 due to less reaction steps and lower overall barrier from the reactants (R1 and R2) to the final dissociation products (P1 and P2). However, as SO and SO_3^{2-} are unstable and readily to be reoxidized to sulfates under the rich-O_2 condition, the features of SO and SO_3^{2-} were absent in the IR spectra. Though only the gas phase reactions are calculated in the present study, it could provide theoretical supports for the deduction that the presence of SO_2 and sulfates results in the change of the reactions of −CN species to accelerate the production of −NCO species during the SCR reaction. Moreover, it should be noted that the DFT calculations were carried out based on the in situ FTIR observations over the $Cu/Ti_{0.7}Zr_{0.3}O_{2-\delta}$ catalyst, thus the proposed mechanism on the reactions of −CN species in the SO_2-containing SCR reaction is not universal.

3.6. Reaction Mechanism. On the basis of the results of in situ FTIR and DFT calculations, a modified reaction mechanism of C_3H_6-SCR over the $Cu/Ti_{0.7}Zr_{0.3}O_{2-\delta}$ catalyst in the presence of SO_2 is proposed in Scheme 1. Similar to the

Scheme 1. Proposed C_3H_6-SCR Reaction Mechanism over the $Cu/Ti_{0.7}Zr_{0.3}O_{2-\delta}$ catalyst in the Presence of SO_2

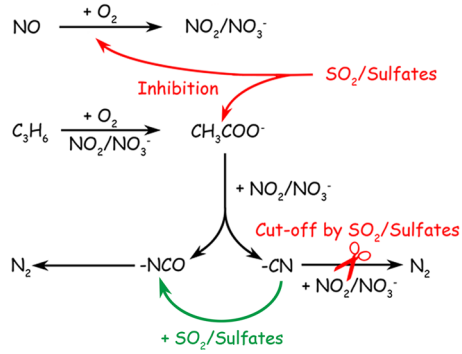

SO_2-free SCR process reported previously,[64] NO and C_3H_6 are oxidized first under an O_2-rich condition forming NO_2 and/or nitrates and oxygenated hydrocarbons (formate, acetate and acetone), and C_3H_6 activation is enhanced by NO_2 and/or nitrates. The presence of SO_2 leads to the deposition of sulfates on the catalyst surface, and the catalyst sulfation results in the weakened adsorption capacity of the catalyst toward nitrates and/or NO_2. Meanwhile, the C_3H_6 activation is also inhibited to some extent and the reduced generation of acetate is considered as one of the important reasons for the activity decline in the temperature range of 150−250 °C due to the high activity of acetate in the reaction with NO_2 and nitrates. When the reaction temperature is up to 275 °C, the negative effect of SO_2 on the formation of acetate is quite weak, and the consequent enhancement of the generation of N-containing

dx.doi.org/10.1021/cs5005739 | ACS Catal. 2014, 4, 2426−2436

organic species promotes the SCR activity. In the SO_2-containing SCR reaction, there is a new pathway for the generation of −NCO species, i.e., the rapid reaction between the −CN species and SO_2 and/or sulfates, which increases the quantity of surface adsorbed −NCO species significantly and therefore promotes the SCR activity. Meanwhile, due to the more feasible reaction −CN + SO_2/SO_4^{2-} → −NCO from the dynamic viewpoint, the reaction between −CN and nitrates and/or NO_2 to form N_2 is prevented and then the −NCO species become the sole final intermediate to generate N_2 over the $Cu/Ti_{0.7}Zr_{0.3}O_{2-\delta}$ catalyst in the SO_2-containing SCR reaction.

CONCLUSIONS

In this work, the effects of SO_2 on a Cu-supported Ti−Zr mixed oxide catalyst ($Cu/Ti_{0.7}Zr_{0.3}O_{2-\delta}$) in C_3H_6-SCR reaction have been elucidated. It is concluded that the activity of SCR reaction in the presence of SO_2 depends on the reaction temperature. The catalytic activity declines in the temperature range of 150−250 °C, while the NO conversion increases slightly at high temperature (above 275 °C).

During the SO_2-containing SCR reaction, the competitive adsorption between SO_2 and NO suppressed the adsorption and activation of NO on the catalyst surface, and the subsequent generation of NO_2 and nitrates. Meanwhile, the generation of acetate at low temperature (150−250 °C) was also inhibited by SO_2 significantly, and the subsequent less generation of −NCO and −CN species was an important reason for the decline of SCR activity. For the high temperature range, the reasons for the activity promotion were as follows: (i) the suppression of acetate formation by SO_2 is quite weak when the reaction temperature was above 275 °C, which benefitted the generation of N-containing organic species; (ii) the rapid reaction between −CN species and SO_2 and/or sulfates accelerates the generation of −NCO species significantly. The introduction of SO_2 prevented the reaction between −CN and NO_2 and/or nitrates, due to the much higher dynamical feasibility of the reaction −CN + SO_2/SO_4^{2-} → −NCO.

ASSOCIATED CONTENT

Supporting Information

Additional details concerning the table of the wavenumbers and assignment of adsorption bands in FTIR spectra, XRD patterns, FTIR spectra of NO + O_2 adsorption, FTIR spectra of C_3H_6 + O_2 adsorption, FTIR spectra of the reaction between −CN species and O_2, and the optimized geometries of reactants, products, intermediates and transition states. This material is available free of charge via the Internet at http://pubs.acs.org.

AUTHOR INFORMATION

Corresponding Author

*X. Li. : Tel: +86-411-8470-7733. Fax: +86-411-8470-7733. E-mail: xinyongli@hotmail.com.

Notes

The authors declare no competing financial interest.

ACKNOWLEDGMENTS

This work was supported financially by the National Nature Science Foundation of China (21377015, 51178076), the Key Laboratory of Industrial Ecology and Environmental Engineering, China Ministry of Education and the Fundamental Research Funds for the Central Universities.

REFERENCES

(1) Oliveira, M. L. M. d.; Silva, C. M.; Moreno-Tost, R.; Farias, T. L.; Jiménez-López, A.; Rodríguez-Castellón, E. *Appl. Catal., B* **2009**, *88*, 420−429.
(2) Shelef, M. *Chem. Rev.* **1995**, *95*, 209−225.
(3) Huo, H.; Zhang, Q.; Liu, F.; He, K. *Environ. Sci. Technol.* **2013**, *47*, 1711−1718.
(4) Lu, G.; Li, X.; Qu, Z.; Zhao, Q.; Zhao, L.; Chen, G. *Chem. Eng. J.* **2011**, *168*, 1128−1133.
(5) Pan, H.; Su, Q.; Chen, J.; Ye, Q.; Liu, Y.; Shi, Y. *Environ. Sci. Technol.* **2009**, *43*, 9348−9353.
(6) Li, X.; Lu, G.; Qu, Z.; Zhang, D.; Liu, S. *Appl. Catal., A* **2011**, *398*, 82−87.
(7) Marnellos, G. E.; Efthimiadis, E. A.; Vasalos, I. A. *Appl. Catal., B* **2004**, *48*, 1−15.
(8) Yang, W.; Zhang, R.; Chen, B.; Duprez, D.; Royer, S. *Environ. Sci. Technol.* **2012**, *46*, 11280−11288.
(9) Gawade, P.; Alexander, A.-M. C.; Silver, R.; Ozkan, U. S. *Energy Fuels* **2012**, *26*, 7084−7091.
(10) Liu, J.; Li, X.; Zhao, Q.; Zhang, D. *Catal. Sci. Technol.* **2012**, *2*, 1711−1718.
(11) Tsoncheva, T.; Gallo, A.; Spassova, I.; Dimitrov, M.; Genova, I.; Marelli, M.; Khristova, M.; Atanasova, G.; Kovacheva, D.; Santo, V. *Appl. Catal., A* **2013**, *464−465*, 243−252.
(12) Kumar, P.; Reddy, M.; Ju, L.; Hyun-Sook, B.; Phil, H. *J. Mol. Catal. A: Chem.* **2008**, *291*, 66−74.
(13) Shibata, J.; Shimizu, K.; Satsuma, A.; Hattori, T. *Appl. Catal., B* **2002**, *37*, 197−204.
(14) Gervasini, A.; Manzoli, M.; Martra, G.; Ponti, A.; Ravasio, N.; Sordelli, L.; Zaccheria, F. *J. Phys. Chem. B* **2006**, *110*, 7851−7861.
(15) Richter, M.; Langpape, M.; Kolf, S.; Grubert, G.; Eckelt, R.; Radnik, J.; Schneider, M.; Pohl, M.-M.; Fricke, R. *Appl. Catal., B* **2002**, *36*, 261−277.
(16) Yang, S.; Guo, Y.; Chang, H.; Ma, L.; Peng, Y.; Qu, Z.; Yan, N.; Wang, C.; Li, J. *Appl. Catal., B* **2013**, *136−137*, 19−28.
(17) Watson, J. M.; Ozkan, U. S. *J. Catal.* **2003**, *217*, 1−11.
(18) Tang, N.; Liu, Y.; Wang, H.; Wu, Z. *J. Phys. Chem. C* **2011**, *115*, 8214−8220.
(19) Doronkin, D. E.; Khan, T. S.; Bligaard, T.; Fogel, S.; Gabrielsson, P.; Dahl, S. *Appl. Catal., B.* **2012**, *117−118*, 49−58.
(20) Bion, N.; Saussey, J.; Haneda, M.; Daturi, M. *J. Catal.* **2003**, *217*, 47−58.
(21) Haneda, M.; Kintaichi, Y.; Inaba, M.; Hamada, H. *Catal. Today* **1998**, *42*, 127−135.
(22) Shimizu, K.; Satsuma, A. *Phys. Chem. Chem. Phys.* **2006**, *8*, 2677−2695.
(23) Shimizu, K.; Higashimata, T.; Tsuzuki, M.; Satsuma, A. *J. Catal.* **2006**, *239*, 117−124.
(24) Park, P. W.; Boyer, C. L. *Appl. Catal., B* **2005**, *59*, 27−34.
(25) Xie, S.; Wang, J.; He, H. *J. Mol. Catal. A: Chem.* **2007**, *266*, 166−172.
(26) Kantcheva, M.; Cayirtepe, I.; Naydenov, A.; Ivanov, G. *Catal. Today* **2011**, *176*, 437−440.
(27) Tsyntsarski, B.; Avreyska, V.; Kolev, H.; Marinova, Ts.; Klissurski, D.; Hadjiivanov, K. *J. Mol. Catal. A: Chem.* **2003**, *193*, 139−149.
(28) Li, J.; Zhu, Y.; Ke, R.; Hao, J. *Appl. Catal., B* **2008**, *80*, 202−213.
(29) Wang, J.; He, H.; Xie, S.; Yu, Y. *Catal. Commun.* **2005**, *6*, 195−200.
(30) Jagtap, N.; Umbarkar, S. B.; Miquel, P.; Granger, P.; Dongare, M. K. *Appl. Catal., B* **2009**, *90*, 416−425.
(31) Sadykov, V.; Kuznetsova, T.; Doronin, V.; Bunina, R.; Alikina, G.; Batuev, L.; Matyshak, V.; Rozovskii, A.; Tretyakov, V.; Burdeynaya, T.; Lunin, V.; Ross, J. *Catal. Today* **2006**, *114*, 13−22.
(32) Pasel, J.; Speer, V.; Albrecht, C.; Richter, F.; Papp, H. *Appl. Catal., B* **2000**, *25*, 105−113.

(33) Komvokis, V. G.; Eleni, E. F.; Vasalos, I. A.; Triantafyllidis, K. S.; Marshall, C. L. *Appl. Catal., A* **2007**, *325*, 345−352.
(34) Houel, V.; James, D.; Millington, P.; Pollington, S.; Poulston, S.; Rajaram, R.; Torbati, R. *J. Catal.* **2005**, *230*, 150−157.
(35) Frisch, M. J.; Trucks, G.. W.; Schlegel, H. B.; Scuseria, G. E.; Robb, M. A.; Cheeseman, J. R.; Scalmani, G.; Barone, V.; Mennucci, B.; Petersson, G. A.; Nakatsuji, H.; Caricato, M.; Li, X.; Hratchian, H. P.; Izmaylov, A. F.; Bloino, J.; Zheng, G.; Sonnenberg, J. L.; Hada, M.; Ehara, M.; Toyota, K.; Fukuda, R.; Hasegawa, J.; Ishida, M.; Nakajima, T.; Honda, Y.; Kitao, O.; Nakai, H.; Vreven, T.; Montgomery, J. A.; Peralta, J. E., Jr.; Ogliaro, F.; Bearpark, M.; Heyd, J. J.; Brothers, E.; Kudin, K. N.; Staroverov, V. N.; Kobayashi, R.; Normand, J.; Raghavachari, K.; Rendell, A.; Burant, J. C.; Iyengar, S. S.; Tomasi, J.; Cossi, M.; Rega, N.; Millam, J. M.; Klene, M.; Knox, J. E.; Cross, J. B.; Bakken, V.; Adamo, C.; Jaramillo, J.; Gomperts, R.; Stratmann, R. E.; Yazyev, O.; Austin, A. J.; Cammi, R.; Pomelli, C.; Ochterski, J. W.; Martin, R. L.; Morokuma, K.; Zakrzewski, V. G.; Voth, G. A.; Salvador, P.; Dannenberg, J. J.; Dapprich, S.; Daniels, A. D.; Farkas, O.; Foresman, J. B.; Ortiz, J. V.; Cioslowski, J.; Fox, D. J. *Gaussian 09*, Revision A.1; Gaussian, Inc., Wallingford, CT, 2009.
(36) Hamill, C.; Burch, R.; Goguet, A.; Rooney, D.; Driss, H.; Petrov, L.; Daous, M. *Appl. Catal., B* **2014**, *147*, 864−870.
(37) Amiridis, M. D.; Roberts, K. L.; Pereira, C. J. *Appl. Catal., B* **1997**, *14*, 203−209.
(38) Flores-Moreno, J. L.; Delahay, G.; Figueras, F.; Coq, B. *J. Catal.* **2005**, *236*, 292−303.
(39) Yan, Y.; Yu, Y.; He, H.; Zhao, J. *J. Catal.* **2012**, *293*, 13−26.
(40) Chansai, S.; Burch, R.; Hardacre, C.; Breen, J.; Meunier, F. *J. Catal.* **2011**, *281*, 98−105.
(41) Chen, L.; Li, J.; Ge, M. *Environ. Sci. Technol.* **2010**, *44*, 9590−9596.
(42) Sun, C.; Zhu, J.; Lv, Y.; Qi, L.; Liu, B.; Gao, F.; Sun, K.; Dong, L.; Chen, Y. *Appl. Catal., B:* **2011**, *103*, 206−220.
(43) Ma, Q.; Liu, Y.; He, H. *J. Phys. Chem. A* **2008**, *112*, 6630−6635.
(44) Nguyen, L. Q.; Salim, C.; Hinode, H. *Appl. Catal., B* **2010**, *96*, 299−306.
(45) Jing, G.; Li, J.; Yang, D.; Hao, J. *Appl. Catal., B* **2009**, *91*, 123−134.
(46) Shimizu, K.; Shibata, J.; Satsuma, A. *J. Catal.* **2006**, *239*, 402−409.
(47) Sazama, P.; Čapek, L.; Drobná, H.; Sobalík, Z.; Dědeček, J.; Arve, K.; Wichterlová, B. *J. Catal.* **2005**, *232*, 302−317.
(48) Szanyi, J.; Kwak, J. H.; Peden, C. H. F. *Phys. Chem. Chem. Phys.* **2013**, *15*, 2368−2380.
(49) Levasseur, B.; Ebrahim, A. M.; Bandosz, T. J. *Langmuir* **2011**, *27*, 9379−9386.
(50) Chi, Y.; Chuang, S. S. C. *J. Catal.* **2000**, *190*, 75−91.
(51) Jiang, B. Q.; Wu, Z. B.; Liu, Y.; Lee, S. C.; Ho, W. K. *J. Phys. Chem. C* **2010**, *114*, 4961−4965.
(52) Liu, F.; He, H. *Catal. Today* **2010**, *153*, 70−76.
(53) Ito, K.; Kakino, S.; Ikeue, K.; Machida, M. *Appl. Catal., B* **2007**, *74*, 137−143.
(54) Pietrzyk, P.; Dujardin, C.; Gora-Marek, K.; Granger, P.; Sojka, Z. *Phys. Chem. Chem. Phys.* **2012**, *14*, 2203−2215.
(55) Liu, Z.; Woo, S. I.; Lee, W. S. *J. Phys. Chem. B* **2006**, *110*, 26019−26023.
(56) Bridier, B.; López, N.; Pérez-Ramírez, J. *J. Catal.* **2010**, *269*, 80−92.
(57) Yu, Y.; Zhang, X.; He, H. *Appl. Catal., B* **2007**, *75*, 298−302.
(58) Yu, Y.; He, H.; Feng, Q.; Gao, H.; Yang, X. *Appl. Catal., B* **2004**, *49*, 159−171.
(59) Long, J.; Zhang, Z.; Ding, Z.; Ruan, R.; Li, Z.; Wang, X. *J. Phys. Chem. C* **2010**, *114*, 15713−15727.
(60) Liu, X.; Wang, A.; Li, L.; Zhang, T.; Mou, C. Y.; Lee, J. F. *J. Catal.* **2011**, *278*, 288−296.
(61) Luo, M. F.; Ma, J. M.; Lu, J. Q.; Song, Y. P.; Wang, Y. J. *J. Catal.* **2007**, *246*, 52−59.
(62) Jia, A. P.; Hu, G. S.; Meng, L.; Xie, Y. L.; Lu, J. Q.; Luo, M. F. *J. Catal.* **2012**, *289*, 199−209.
(63) Yang, W.; Zhang, R.; Chen, B.; Bion, N.; Duprez, D.; Royer, S. *J. Catal.* **2012**, *295*, 45−58.
(64) Liu, J.; Li, X.; Zhao, Q.; Hao, C.; Zhang, D. *Environ. Sci. Technol.* **2013**, *47*, 4528−4535.
(65) Watanabe, S.; Ma, X.; Song, C. *J. Phys. Chem. C* **2009**, *113*, 14249−14257.
(66) Liu, F.; He, H.; Ding, Y.; Zhang, C. *Appl. Catal., B* **2009**, *93*, 194−204.
(67) Feng, W.; Hershberger, J. F. *J. Phys. Chem. A* **2011**, *115*, 286−290.